Vestibular CCK neurons drive motion-induced malaise

Pablo Machuca-Márquez[1], Laura Sánchez-Benito[1,2], Fabien Menardy[1], Andrea Urpi[1], Isabella Appiah[1], Richard Palmiter[3], Elisenda Sanz[1,2*], Albert Quintana[1,2*]

Affiliations

1) Institut de Neurociències, Universitat Autònoma de Barcelona. Bellaterra (Barcelona) 08193. Spain
2) Department of Cell Biology, Physiology, and Immunology Universitat Autònoma de Barcelona. Bellaterra (Barcelona) 08193. Spain
3) Howard Hughes Medical Institute and Department of Biochemistry, University of Washington, Seattle WA 98195

*These authors have jointly supervised the work

Corresponding author: elisenda.sanz@uab.cat; albert.quintana@uab.cat

ABSTRACT

Passive motion can induce kinetosis (motion sickness, MS) in susceptible individuals. MS is an evolutionary conserved mechanism caused by mismatches between motion-related sensory information and past visual and motion memory, triggering a malaise accompanied by hypolocomotion, hypothermia, hypophagia and aversion to novel foods presented coincidentally. Vestibular nuclei (VN) are critical for the processing of movement input, and motion-induced activation of VN neurons recapitulates MS-related signs. However, the genetic identity of VN neurons mediating MS-related autonomic and aversive responses remains unknown. Here, we identify a glutamatergic vestibular circuitry necessary to elicit MS-related behavioral responses, defining a central role of cholecystokinin (CCK)-expressing glutamatergic VN neurons in vestibular-induced malaise. Moreover, we show that CCK VN inputs onto the parabrachial nucleus activate *Calca*-expressing neurons and are sufficient to establish hypothermia and aversion to novel food. Together, we provide novel insight into the neurobiological regulation of MS, unravelling key genetically defined neural substrates for kinetosis.

INTRODUCTION

Motion sickness (MS) is an unpleasant autonomic physiological alteration that occurs in healthy individuals undergoing passive or even illusory motion. MS signs and symptoms include pallor, cold sweating, yawning, retching and vomiting, vertigo, anorexia, drowsiness, and even severe pain[1-5]. MS is highly conserved among species[4, 6-9]. Thus, while still debated[10], it has been posited that MS may provide an evolutionary benefit acting as an early warning system leading to a metabolic expense reduction (hypothermia and drowsiness), expulsion of the toxin (vomiting) and future avoidance (taste aversion) of the ingested substance[6].

It is widely accepted that MS arises from conflicts between actual visual/vestibular sensory inputs and the expected motion and body position information based on past memories[11-13]. Accordingly, the necessity of a functional vestibular system for the development of MS was identified long ago[14, 15]. Movement-related information processed by the vestibular organ in the inner ear is relayed directly to the medullo-pontine vestibular nuclei (VN). Compelling evidence demonstrates that VN neurons are particularly crucial in MS neurobiological regulation by showing that activation of VN neurons through provocative motion reproduced MS-like autonomic alterations in rats and mice[16, 17]. In addition, diseases caused by VN affectation are associated to autonomic dysregulation such as vertigo, nausea, and vomiting[18].

The role of the VN in the control of the body orientation system, mainly by means of vestibular reflexes at the ocular, head, neck, and spinal levels, has been amply described[19]. Furthermore, vestibular outputs have been shown to modulate blood pressure with posture change[20, 21]. However, how vestibular function governs motion-induced changes in other MS-mediated responses, such as hypolocomotion, appetite suppression, loss of body temperature, or acquisition of a conditioned taste aversion (CTA)[3, 4, 8, 16, 17, 22-24], is still unknown. In this regard, mapping of neuronal activity after provocative motion has identified

potential neural substrates for vestibular-induced physiological responses, such as the Nucleus of the Solitary Tract (NTS), paraventricular nucleus of the hypothalamus (PVN), parabrachial nucleus (PBN), central amygdala (CeA), dorsal raphe nucleus, locus coeruleus and area postrema[16, 17]. Among them, both the NTS and PBN are known to process visceral sensory input in the brainstem[25] and receive direct connections from the VN[26, 27].

Excitatory neurons are the main projection-neuron type in the VN[28] and have been suggested to participate in autonomic responses after hypergravity[29]. Furthermore, provocative-motion stimuli activate glutamatergic vesicular glutamate transporter 2 (VGLUT2)-expressing VN neurons that in turn project to downstream nuclei such as the PBN[30-32]. Thus, we hypothesized that genetically defined, glutamatergic neuronal (sub)populations and circuits in the VN are sufficient and/or necessary to develop MS-induced autonomic regulation and/or aversive learning. To that end, we used cell-type-specific transcriptomics combined with optogenetic and chemogenetic approaches to identify the underlying vestibular circuitry of MS-induced responses.

RESULTS

Glutamatergic vestibular neurons sustain motion-induced autonomic responses

Assessment of MS in mice is hindered by the lack of emetic reflex and difficulty to unequivocally identify nausea[5, 8, 33]. However, behavioral and autonomic signs of MS are consistently observed in mice subjected to rotatory or gravitational paradigms[8, 16, 17]. Thus, we sought to establish a rotational paradigm sufficient to robustly develop MS-like signs (Fig. 1a). Consistently, four repeated 1-min 4 *g* accelerations (spin stimulation) induced transient hypolocomotion (Fig. 1b and Extended Data Fig. 1a). Furthermore, a significant decrease in food intake was observed in food-deprived mice after spin stimulation

compared to controls (Fig. 1c), in line with the appetite suppression observed in MS[3, 4, 8, 16, 23]. In addition, a decrease in core body temperature, another classical MS response[3, 4, 8, 17, 23, 24], was observed after the rotational stimulus compared to controls, with a maximum temperature difference of 4°C that occurred ~17.5 min after rotation onset (Fig. 1d).

With the validity of the rotation paradigm established, we set out to define the neuronal substrate of vestibular-induced, MS-like responses. Excitatory neurons are highly abundant in the VN[28] and glutamatergic VN neurons are activated after provocative motion[32]. Among the different glutamatergic markers, VGLUT2 (encoded by *Slc17a6*) shows a robust and significant expression in the VN[34], and VGLUT2-expressing neurons have been shown to participate in vestibular responses to hypergravity, in contrast to VGAT-expressing inhibitory neurons[29]. Thus, we assessed the necessity of genetically defined glutamatergic VGLUT2-expressing VN ($VGLUT2^{VN}$) neurons in eliciting MS behavioral and autonomic responses by bilateral chemogenetic inhibition in a well-characterized *Slc17a6*^{Cre} mouse line[35] (Fig. 1e). Correct targeting of $VGLUT2^{VN}$ neurons expressing hM4Di-mCherry was subsequently verified by immunofluorescence (IF) analysis using an anti-mCherry antibody (Extended Data Fig. 1b). Targeted inhibition of $VGLUT2^{VN}$ neurons did not induce significant effects on locomotion prior to spin stimulation (Extended Data Fig. 1c). However, inhibition of $VGLUT2^{VN}$ neurons by addition of the clozapine N-oxide (CNO) ligand prevented spin-induced decreases in ambulatory activity (Fig. 1f), appetite suppression (Fig. 1g) and attenuated the MS-related decrease in body temperature (Fig. 1h). Noteworthy, an initial decrease in body temperature was observed in CNO-injected mice (Fig. 1h), suggesting that other neuronal populations may contribute to the early spin-induced drop in body temperature. These results indicate that $VGLUT2^{VN}$ neurons are necessary to promote the development of the MS-like behavioral and autonomic responses elicited by rotational stimulation.

Nauseogenic responses can be obtained after unilateral inner ear caloric

stimulation[36]. Hence, to test whether VGLUT2^{VN} neuronal activation is sufficient to induce MS-like autonomic responses, *Slc17a6*^{Cre} mice received a unilateral injection of an AAV1 expressing Cre-dependent ChR2·YFP (Vglut2^{VN}:ChR2 mice; for photoactivation) or a YFP construct (Vglut2^{VN}:YFP mice; as control) into the right VN and an optical fiber was implanted over the injected VN (Fig. 2a). Specific targeting of the viral vector and optical fiber placement were confirmed at the end of the experiment using anti-GFP and anti-GFAP antibodies (Extended Data Fig. 2a). GFP antibodies reveal the transduced cells while the GFAP antibodies reveal astrocyte reactivity resulting from optical fiber implantation. Increasing photostimulation frequencies reduced ambulatory activity in Vglut2^{VN}:ChR2 mice relative to controls (Extended Data Fig. 2b). We used a 5-min, 40-Hz, optogenetic-stimulation paradigm because we and others have shown VGLUT2^{VN} neurons in actively moving mice maintain firing rates of ~40 Hz[37, 38] (Extended Data Fig. 2b). VGLUT2^{VN} neuron optogenetic activation led to a significant decrease in spontaneous ambulatory activity (Fig. 2b), consistent with the results obtained after rotational stimulus. Furthermore, ingestion of their regular, low-calorie chow and water intake after optogenetic VGLUT2^{VN} activation were significantly decreased, showing complete suppression for as long as 30 min after laser onset (Fig. 2c, d). Noteworthy, a recovery in the feeding pattern was observed after presentation of highly palatable, chocolate-flavored, liquid diet to a separate cohort of laser-stimulated Vglut2^{VN}:ChR2 mice (Fig. 2e), ruling out physical inability to feed but rather a lack of motivational drive to consume regular chow or water. Core body temperature significantly decreased, with a maximum 3°C-drop occurring 17.5 min after laser onset (Fig. 2f). To rule out the possibility that optogenetic-induced loss of core body temperature was due to a reduction in ambulatory activity in Vglut2^{VN}:ChR2 mice, an additional optogenetic stimulation was applied under physical restraint. Under these conditions, core body temperature increased in Vglut2^{VN}:YFP mice, likely due to restraint-induced stress responses. However, Vglut2^{VN}:ChR2 mice still showed a significant drop in body temperature coincident with

photostimulation (Fig. 2g). These results highlight a role of VGLUT2^{VN} neurons in MS regulation.

Identification of CRH- and CCK-expressing VGLUT2^{VN} neuronal subpopulations

To define VGLUT2^{VN}-neuron subpopulations, we performed viral vector-mediated RiboTag molecular profiling[39-41] in VN homogenates of *Slc17a6^{Cre}* mice injected with a RiboTag-expressing construct (AAV1-DIO-Rpl22·HA[40], Fig. 3a). Transcripts enriched in VGLUT2^{VN} neurons were identified by differential expression analysis in RNA samples extracted from the RiboTag immunoprecipitates (IP; containing polysome-associated mRNAs from VGLUT2^{VN} neurons) and the input (I) of the immunoprecipitation (containing RNA from all the different cell types in the VN). Data analysis confirmed specific enrichment for *Slc17a6* (Vglut2), and depletion for inhibitory neuron (*Gad2*) and non-neuronal marker transcripts (*Cnp*, *Gfap*) in the RiboTag IPs, and revealed significant enrichment for candidate VGLUT2^{VN} neuron subpopulation markers such as *Cck*, *Crh*, *Adcyap1*, *Gal* and *Coch* (Fig. 3b). Among these, *Crh*- and *Cck*-expressing neurons have been shown to be involved in autonomic and nauseogenic responses[42, 43], highlighting the potential relevance of these neuronal populations in VN-mediated MS responses. Subsequent *in situ* hybridization assays confirmed co-localization of either *Crh* or *Cck* with *Slc17a6* (Fig 3c, g).

Modulation of vestibular CCK-expressing neurons causes MS-like autonomic responses

To test the necessity of vestibular *Crh*- or *Cck*-expressing neuronal populations (CRH^{VN} or CCK^{VN} neurons, respectively) in the development of MS-like signs, we injected *Crh^{Cre}* or *Cck^{Cre}* mice bilaterally in the VN with a AAV vector carrying Cre-dependent hM4Di-mCherry (Fig. 3d, h). Chemogenetic inhibition of CRH^{VN} neurons did not induce any effect pre- or post-spin on ambulatory activity (Extended Data Fig. 3a and Fig. 3e) or core body

temperature changes (Fig. 3f) compared to vehicle-treated mice, indicating that they are not necessary to develop rotation-induced autonomic responses. Noteworthy, optogenetic stimulation of CRH^{VN} neurons (Extended Data Fig. 3b) induced a marked reduction in locomotion and body temperature (Extended Data Fig. 3c, d), suggesting that this neuronal population is sufficient, but not necessary, to induce MS-like symptoms. On the other hand, bilateral chemogenetic inhibition of CCK^{VN} neurons significantly decreased ambulatory activity in the absence of rotational stimulus (Fig. 3i), which led to an inability to move after the spin (Fig. 3j). Thus, CCK^{VN} inhibition *per se* is sufficient to induce locomotor effects. Core body temperature also decreased in the CNO-injected hM4Di group, dropping >4°C compared to vehicle-injected mice (Fig. 3k) and exacerbated by rotational stimulation (Fig. 3l). Subsequently, we performed optogenetic activation of CCK^{VN} neurons (Fig. 4a, b), which led to a significant and prolonged decrease in spontaneous ambulatory activity in the open-field test compared to the control animals (Fig. 4c). Similarly, food intake was significantly decreased after photostimulation of CCK^{VN} neurons, showing a complete suppression for 35 min, while control animals engaged in feeding almost immediately (Fig. 4d). Optogenetic stimulation of CCK^{VN} neurons reduced core temperature (~4.5°C), occurring 22.5 min after laser onset, in contrast with control mice (Fig. 4e). These results underscore the role of CCK^{VN} neuronal activity in mediating MS-like behavioral and autonomic responses.

CCK^{VN} neurons send dense projections to the PBN

Because optogenetic activation of $VGLUT2^{VN}$ or CCK^{VN} neurons elicits similar behavioral responses, we hypothesized that common projection areas between the two populations would underlie these MS-like responses. To elucidate the genetically defined, vestibular circuits involved in these responses, *Slc17a6*^{Cre} or *Cck*^{Cre} mice received a unilateral injection of an AAV1 expressing a Cre-dependent synaptophysin·GFP fusion protein[44] in the right VN to identify both unilateral and contralateral projection regions for each neuronal population

(Fig. 5a, c). Among the different targeted areas, dense VGLUT2^{VN} and CCK^{VN} terminals were found in the ipsilateral PBN (Fig. 5b, d), with much less intense projections to the contralateral PBN (data not shown). These results suggested that a *Slc17a6*- and *Cck*-expressing vestibulo-parabrachial (CCK$^{VN\rightarrow PBN}$) circuit might be relevant in MS.

CCK$^{VN\rightarrow PBN}$ circuit stimulation mediates MS-induced hypothermia

To ascertain whether the CCK$^{VN\rightarrow PBN}$ circuit plays a role in MS-like behavioral and autonomic symptoms, we optogenetically activated CCK^{VN} axon terminals in the PBN by placing the optical fiber-tip over this region in Cck^{VN}:ChR2 mice (Fig. 5e). After behavioral testing, the presence of ChR2·YFP-positive terminals and successful optical fiber placement in the PBN was verified (Extended Data Fig. 4a). This analysis also revealed projections of CCK^{VN} neurons to the NTS (Extended Data Fig. 4b). Behaviorally, optogenetic stimulation of CCK$^{VN\rightarrow PBN}$ fibers did not lead to significant differences in locomotion or food intake (Fig. 5f, g). However, a significant decrease in body temperature was observed after optogenetic stimulation of this circuit (Fig. 5h). Overall, these results suggest an involvement of the CCK$^{VN\rightarrow PBN}$ circuit in MS-related body temperature regulation, likely in coordination with CCK^{VN} projections to other brain regions.

A CCK$^{VN\rightarrow PBN}$ circuit stimulation mediates MS-like CTA response

MS is known to induce a robust CTA[22], which has been proposed to be a byproduct of a defense system[6], and the PBN has been shown to mediate MS-like CTA acquisition[45]. Hence, we asked whether the CCK$^{VN\rightarrow PBN}$ circuit can establish a CTA. We adapted a two-bottle CTA test[46] (Fig. 6a). Two conditioning sessions paired a 5% sucrose solution with rotational motion, followed by a choice test the next day of water or sucrose. We observed a significant reduction in sucrose preference when sucrose was paired with rotation, compared to controls (Fig. 6b), in agreement with the role of MS establishing a CTA[22]. Pairing sucrose

with optogenetic activation of the CCK^{VN} subpopulation by placing the fiber-optic over either the VN or the projection to the PBN also significantly decreased sucrose preference when compared to controls (Fig. 6c, d). Pairing of the 5% sucrose solution to unilateral optogenetic activation of the YFP-control group did not result in CTA. Consistent with these results, inhibition $VGLUT2^{VN}$ neurons by expression of hM4Di and administration of CNO prevented spin-induced CTA (Fig. 6e). However, pairing 5% sucrose solution to unilateral optogenetic activation of $VGLUT2^{VN}$ neurons did not result in significant differences between the ChR2 and the YFP group (Fig. 6f). These results reveal that activation of CCK^{VN} neurons that project to the PBN is sufficient to develop MS-like CTA and activation of $VGLUT2^{VN}$ neurons is necessary for development of MS-induced CTA.

To identify the neuronal population in the PBN receiving inputs from CCK^{VN} neurons, we performed double-label ISH assays for *Fos* (a marker of neuronal activity) and *Calca* (encodes calcitonin gene-related peptide, CGRP) because these PBN neurons have been implicated in mediating visceral malaise and CTA[44, 47, 48]. Photoactivation of CCK^{VN} neurons increased the number of *Fos* positive-cells in the PBN, which colocalized in part to *Calca*-expressing neurons (Fig. 6g). Importantly, rotational stimulation also induced *Fos* in *Calca*-expressing cells, supporting a role for this neuronal population in mediating MS-induced CTA (Extended Data Fig. 5a). These results underscore $CCK^{VN \rightarrow PBN}$ activation of CGRP neurons as a key component of MS-induced CTA.

DISCUSSION

MS has long accompanied and disabled humans. Being described by Hippocrates over 2000 years ago, MS has affected millions of individuals, including historical figures such as Julius Caesar and Charles Darwin[3]. The CNS is thought to compute an MS-triggering sensory

conflict signal analogously to “toxic shock”, eliciting malaise and nausea[6, 12, 24, 49]. Thus, in an evolutionary context, MS responses could represent a proxy for toxicity-induced balance mismatches. Hence, vomiting observed in humans would be a response to evacuate toxic substances, appetite suppression to avoid additional toxic ingestion, hypolocomotion and hypothermia to minimize the metabolism, and CTA to avoid consumption of toxins in the future. However, the neurobiological underpinnings of MS have remained elusive. Our results link VGLUT2^{VN} and CCK^{VN} excitatory neuronal populations to the development of MS-like symptoms in mice. Furthermore, we show that CCK$^{VN \rightarrow PBN}$ projections are sufficient to induce hypothermia and CTA, common features of MS, likely through the activation of CGRP^{PBN} neurons (Fig. 7).

MS is conserved among animal phyla[4, 6-9], but with a high degree of heterogeneity in its behavioral and physiological correlates. Mice do not present an emetic reflex but do present overt physiological and behavioral alterations when exposed to a nauseogenic experience[4, 17, 22, 23] such as sustained 2 *g* rotational stimuli[8, 16, 17, 23, 29]. We show that a rotational stimulus of 4 min is sufficient to develop robust hypolocomotion, hypophagia, hypothermia, and CTA to a novel food.

The role of the VN in the development of MS is well recognized[16, 17]. The currently accepted hypothesis is that the vestibular inner ear organs provide a major input for the subsequent computing comparisons between present sensory input (integrated input including vestibular, visual and proprioceptive information) and memory recalled from similar motion situations experienced in the past[12, 13]. Rotational stimuli convey information from the semicircular canals mostly onto medial VN (MVN) neurons, leading to nauseogenic responses[5, 36, 50]. Here we show that optogenetic activation of VGLUT2^{VN} neurons that are abundant in the VN[16, 28, 32, 34, 51] is sufficient to induce MS-like behaviors such as hypolocomotion, hypothermia and hypophagia, in agreement with recent results[29]. Furthermore, our bilateral chemogenetic inhibition experiments show, for the first time, that

VGLUT2^{VN} neurons are necessary for the development of MS responses in a rotational paradigm in mice.

Several excitatory populations have been described in the VN that may be involved in different aspects of vestibular-mediated responses[51]. Using the RiboTag approach[39] we identified several genetic markers for subpopulations. Our results validate genes *Crh* and *Adcyap1*[51] and identify new markers for VGLUT2^{VN} neurons including *Gal*, *Coch* and *Cck*. We show a differential role for CCK^{VN} and CRH^{VN} in the appearance of MS-like behaviors. Unilateral optogenetic activation of either CCK^{VN} or CRH^{VN} neurons is sufficient to induce hypolocomotion, hypothermia and hypophagia. However, CRH^{VN} neurons are not necessary for these MS-like responses after a rotational stimulus, indicating they may be upstream of the effector VGLUT2^{VN} subpopulation(s). On the other hand, restricted inhibition of CCK^{VN} neurons significantly decreased ambulatory activity and temperature, even in the absence of a rotational stimulus. Thus, our data show that alterations in the activity of these neurons exert a pivotal role in controlling MS-like behavioral responses. MVN neurons produce endogenous, spontaneous pacemaker activity[52]. Restoration of MVN pacemaker activity is key for MS habituation[53]. Thus, CCK^{VN} neurons may contribute to pacemaker activity and variations of their rhythmic firing rate may lead to MS-like symptoms.

We validated dense projections from VGLUT2^{VN} and CCK^{VN} neurons to the PBN[32]. The PBN is known to mediate malaise, appetite suppression, lethargy, anxiety, thermoregulation, and CTA[25, 54]. Chemogenetic inhibition of VGLUT2^{VN} neurons blocked hypothermia and CTA in our MS paradigm. Unilateral optogenetic stimulation of CCK^{VN} neurons or the projection to the PBN produced hypothermia and robust CTA. However, optogenetic stimulation of VGLUT2^{VN} neurons was not sufficient to develop CTA, likely suggesting the existence of opposing VGLUT2^{VN} subpopulations. Rotational stimulus and CCK^{VN} optogenetic stimulation activated CGRP-expressing, glutamatergic neurons in the lateral PBN, which are known to be involved in malaise, and CTA[25], sustaining the

establishment of aversive taste memories[46]. Thus, we propose that glutamatergic CCK^{VN} input onto $CGRP^{PBN}$ neurons mediates MS-induced CTA. Activation of $VGLUT2^{VN}$ neurons leads to hypothermia, likely by decreasing sympathetic tone[29]. Recent reports revealed that *Pdyn*-expressing PBN neurons ($Pdyn^{PBN}$) regulate hypothermia through projections to the pre-optic area[54], involved in temperature regulation[55]. Hence, CCK^{VN} activation of $Pdyn^{PBN}$ neurons might mediate the MS-induced drop in body temperature. $CCK^{VN \rightarrow PBN}$ projections do not seem to participate in MS-induced hypophagia and hypoactivity, even though activation of $CGRP^{PBN}$ neurons is involved in appetite suppression and reduced locomotion[25, 44]. Thus, it is likely that CCK^{VN} projections to other brain areas may be responsible for these responses. For example, CCK^{VN} neurons also project to the NTS where neurons reside that can activate PBN^{CGRP} neurons to promote anorexia[56].

Our study underscores a key role for excitatory $VGLUT2^{VN}$ and CCK^{VN} neurons in MS-related behavioral and physiologic responses. Future studies detailing the behavioral and physiological contribution of other CCK^{VN} targets as well as other $VGLUT2^{VN}$ subpopulations will provide a complete profile of the neurobiological substrates of MS.

METHODS

Mice

The following mouse lines were used in this study: $Slc17a6^{Cre}$ (BAC-Vglut2::Cre)[35] mice were generated by Ole Kiehn. Cck^{Cre} (CCK-IRES-Cre) and Crh^{Cre} (CRH-IRES-Cre)[57] mice were obtained from The Jackson Laboratory (Bar Harbor, ME. Stock No: 012706 and 012704, respectively). Mice were group-housed with a 12:12h light:dark cycle at 22°C, with *ad libitum* access to rodent chow (Teklad Global Rodent Diet #2014S; Envigo) and water, unless otherwise stated. Sex and age-balanced groups of 2- to 7-month-old mice were used across

all experimental procedures. No sex differences were observed. After surgeries, animals were individually housed until the end of all experimental procedures. Sample sizes were determined using power analyses. Number of animals used per experiment (n) are detailed in figure legends. All mice were on a C57BL/6J background after backcrossing for at least 10 generations. All experiments were conducted following the recommendations in the Guide for the Care and Use of Laboratory Animals and were approved by the Animal Care and Use Committee of the Universitat Autònoma de Barcelona and the Generalitat de Catalunya.

Rotational stimulus

Prior to rotational stimulation, animals were habituated to physical restraint for 4 min using a 50-mL conical tube coupled to a custom-made rotary device (external radius: 10.5 cm; internal radius from mouse head: 5 cm. Rotation multiplier: x3.6). Afterwards, rotational (four repeated 1-min, 4-*g* accelerations) or control (4 min with no rotation) stimuli were applied, unless otherwise stated. 1-min accelerations included 55 s of rotation plus 5 s break until full stop. To achieve 4 *g* accelerations, 75 rpm were applied.

Behavioral assays

Each animal was subjected to an open-field test, followed by food intake and conditioned taste aversion (CTA) analysis. After tests, telemetric temperature sensors were implanted, and core-body temperature monitored.

Open-field test

The open-field (OF) test was conducted in a non-covered, white methacrylate box (56 x 36.5 x 31 cm) that allows for video recording during animal testing. Mice were individually exposed for 5 min to the OF before receiving rotational or control stimulation. After stimulation, mice were re-exposed to the OF for 60 more min. For optogenetic experiments,

mice were exposed for a total of 60 min to the OF (5 min of pre-stimulation, followed by 5 min of laser stimulation and 50 min of post-stimulation). Spontaneous ambulatory activity was monitored using a video tracking software (Ethovision XT 11.5; Noldus Information Technology).

Appetite-suppression test

Animals were individually placed in an Oxyletpro-Physiocage monitoring system (Panlab) for real-time quantification of food and liquid intake. Mice were habituated to the cage for 2 to 4 days with *ad libitum* access to normal chow and water, unless otherwise stated. Prior to each session, animals were food deprived for 24 h and refed at the onset of the dark cycle. For specific experiments, chocolate-flavored, highly palatable liquid diet (ENSURE Nutrivigor, Abbott) was provided during cage habituation and in the subsequent experimental sessions. Food and liquid intake were expressed as cumulative intake using the Metabolism software version v3.0.00 (Panlab).

Conditioned taste aversion (CTA) test

For the CTA test, a two bottle-based protocol was used[46]. Animals were individually placed in a custom cage with angular ports for two liquid-containing bottles. *Ad libitum* water access was provided for 2 days during habituation. Next, animals only had access to both water-containing bottles during restricted time periods (30 min access in the morning, 30-60 min in the afternoon) for 8 days (D1- D8). During days 4 and 6 (D4 and D6), a solution of 5% sucrose in water was paired with specific stimuli (rotation, CNO injection, photostimulation) to stablish conditioning. Mice were tested on D8. Sucrose preference value was calculated as sucrose solution consumption/total liquid consumption.

Surgical implantation of telemetry devices and temperature monitoring

Anesthetized mice (5% isoflurane for induction, 1.5% for maintenance) were aseptically implanted with telemetric temperature transmitters (G2 E-Mitter, STARR Life Sciences Corp.) into the peritoneum and allowed to recover for 2 weeks. Mouse cages were placed on telemetry receivers (ER4000 Energizer/Receiver, STARR Life Sciences Corp.) and core body temperature was monitored using the VitalView software version 5.0 (STARR Life Sciences Corp.) under controlled ambient temperature (22°C). All recordings started in resting animals. For specific experiments, mice were inserted into a modified 50-mL Falcon tube to ensure physical restrain while allowing optogenetic tethering.

Viral vector production

pAAV-hSyn-DIO-hM4Di:mCherry, pAAV-EF1a-DIO-eYFP and pAAV-EF1a-DIO- ChR2:YFP plasmids were obtained from Addgene (#44362, #27056 and #100056, respectively). pAAV RiboTag virus (pAAV-EF1a-DIO- Rpl22·HA) and pAAV-EF1a-DIO-Synaptophysin:GFP (Syn·GFP) viruses have been described[40,44]. Recombinant adeno-associated viral vectors (AAV) were produced in human embryonic kidney (HEK293T) cells with AAV1 coat serotype. Purification was achieved by several sucrose and CsCl gradient centrifugations and a final re-suspension in 1x Hanks Balanced Saline Solution (HBSS) at a titer of 2 x 10^9 viral genomes/µL as described[40, 58]. AAV preparations were aliquoted and stored at -80°C until stereotaxic injection.

Stereotaxic surgery

All surgeries were performed under aseptic conditions. Animal anesthesia was induced and maintained with 5% and 1-1.5% isoflurane/O_2, respectively. Analgesia (5 mg/kg ketoprofen; Sanofi-Aventis) and ocular protective gel (Viscotears®, Bausch+Lomb) were applied. Mice were then placed over a heating pad in a robot-operated, 3-dimensional (stereotaxic) frame

(Neurostar) for intracerebral virus delivery. Stereotaxic coordinates were normalized using a correction factor (Bregma-Lambda distance/4.21) based on the coordinates of Paxinos and Franklin[59]. AAV preparations were unilaterally (right side) or bilaterally delivered into the VN (antero-posterior (AP), −5.65 mm; medio-lateral (ML), ± 0.90 mm; dorso-ventral (DV), −4.60 mm from Bregma) at a constant rate of 0.1 µL/min for 3.5-4.0 min (0.35-0.40 µL per injection site) using a 32-guage blunt needle coupled to a 5 µL-syringe (Hamilton). After infusion, the needle was maintained in place for 6 min to allow proper diffusion. Subsequent needle withdrawal was performed at 1 mm/min to ensure minimal off-target viral leakage.
After viral injection, mice used for optogenetic experiments also received unilateral surgical implantation of a fiber-optic cannula as described below.

Chemogenetics

Slc17a6^{Cre}, *Cck*^{Cre} or *Crh*^{Cre} mice were bilaterally injected in the VN with 0.35 µL (per side) of AAV1-hSyn-DIO-hM4Di:mCherry. Clozapine-n-oxide (CNO; 1 mg/kg) was administered via intraperitoneal (i.p.) injection 35 min prior to rotational or control stimulation.

Optogenetics

Slc17a6^{Cre}, *Cck*^{Cre} or *Crh*^{Cre} mice were injected in the right VN with 0.4 µL of either AAV1-EF1α-DIO-ChR2·YFP or AAV1-EF1α-DIO-eYFP and a fiber-optic cannula (200-µm fiber core diameter, 0.22-numeric aperture; 2.5-mm ferrule diameter; Thorlabs) was implanted over the right VN (AP, −5.65 mm; ML, +0.90 mm; DV, -3.80 mm) or over the right PBN (AP, −4.65 mm; ML, +1.70 mm; DV, -3.00 mm) of *Cck*^{Cre} animals. A fiber-optic cannula was fixed to the exposed skull with a layer of adhesive cement (Super-Bond C&B, Sun Medical) and dental acrylic cement (Rebaron, GC Corporation). The skin was affixed to the cement with tissue adhesive (Vetbond, 3M). A blue 473-nm laser light was produced by a DPSS Laser System (LRS-0473-GFM-00100-05 Laserglow) and driven by a fiber-optic patch cord (200-

μm core diameter, 0.22-numeric aperture: FT030 protection, Thorlabs). Light intensity was set at 10 mW measured by a photometer (Thorlabs) at the tip of a non-implanted fiber optic cannula attached to the patch-cord. To deliver illumination to the right VN or right PBN, the patch cord was connected to the implanted fiber-optic-containing cannula through a ceramic sleeve. A pulse generator (33500B Series Trueform, Keysight) was used to adjust laser output to deliver 40-Hz, 10-ms, pulse trains for 5 min to all mice.

Mapping of neuronal projections

To visualize the presynaptic terminals of VGLUT2^{VN} or CCK^{VN} neurons, *Slc17a6*^{Cre} or *Cck*^{Cre} mice were injected into the right VN with 0.35 μL of AAV1-EF1α-DIO-Synaptophysin:GFP[44]. Animals were euthanized 3 weeks after surgery for subsequent immunofluorescence analysis using an anti-GFP antibody as described below.

Tissue processing and Immunofluorescence analysis

Mouse brains were freshly dissected following euthanasia by CO_2 asphyxia, fixed overnight with phosphate-buffered saline (PBS) containing 4% paraformaldehyde (PFA) and cryo-protected with 30% sucrose in PBS. For cryo-sectioning, brains were frozen for 5 min in dry ice and sectioned in a freezing microtome. For immunofluorescence, 30-μm free-floating sections were blocked in PBS with 10% normal donkey serum (NDS) and 0.1% Triton X-100 for 1 h at room temperature followed by an overnight incubation at 4ºC with primary antibody solution containing a chicken anti-GFP (1:2000; #ab13970, Abcam), a rabbit anti-mCherry (1:2000; #ab167453, Abcam) or a rabbit anti-GFAP antibody (1:1000; #PA1-10019, Invitrogen) in PBS with 1% NDS and 0.1% Triton X-100. After three washes in PBS with 0.1% Triton X-100, a secondary antibody solution containing secondary antibodies conjugated to Alexa Fluor fluorophores (1:500; Invitrogen) was added to the sections and incubated for 1 h at room temperature. After the incubation, sections were washed three

times for 5 min in PBS with 0.1% Triton X-100 and mounted onto slides with DAPI Fluoromount (#17984-24, Electron Microscopy Sciences) before visualization with an EVOS imaging system (Thermo Fisher Sci).

RiboTag assays

For genetic identification of neuronal subsets, *Slc17a6*^{Cre} mice were bilaterally injected in the VN with 0.4 µL of the RiboTag viral vector (AAV1-DIO-Rpl22HA)[40]. Animals were euthanized 3 weeks after surgery for subsequent RiboTag analysis. To isolate the polysome-associated mRNAs from VGLUT2^{VN} neurons, punches containing the VN of *Slc17a6*^{Cre} mice injected with AAV1-DIO-Rpl22·HA were pooled and homogenized in 1 ml of buffer as described[41]. After centrifugation, 4 µL of anti-HA antibody (MMS-101R, 2–3 mg/ml; Covance) was added to 800 µL of the cleared lysate and incubated for 4 h at 4°C. Remaining lysate was saved as input sample. After incubation, 200 µL of protein A/G magnetic beads (Thermo Scientific) were added and incubated overnight at 4°C with rotation. Immunoprecipitates (IPs) were washed in high-salt buffer and RNA from inputs and IPs were extracted[39]. For differential expression analysis, 10 ng of RNA was amplified using the Ovation Pico SL WTA system (NuGEN). Fidelity of amplification was confirmed by qPCR analysis of the resulting cDNA using the QuantiTect kit (Qiagen) before biotinylation according to the EncoreIL biotinylation kit (NuGEN). Biotinylated cDNA was quantified, and product size distribution was analyzed using the 2100 Bioanalyzer system with the RNA 6000 Nano chips (Agilent Technologies). Biotinylated cDNA (750 ng) was hybridized at 48°C to MouseRef-8 v2 expression beadchips (Illumina) for 16 h before washing and analyzing according to the manufacturer's directions. Signal was detected using a BeadArray Reader (Illumina), and data were analyzed for differential expression using the GenomeStudio data analysis software (Illumina). Average normalization, the Illumina custom error model, and multiple testing corrections using the Benjamini-Hochberg false discovery rate were applied to the analysis. Only transcripts with a

differential score of >13 ($p < 0.05$) were considered. Normalized and raw data have been deposited in the National Center for Biotechnology Information Gene Expression Omnibus and are accessible through GEO Series accession number GSE167672 (https://www.ncbi.nlm.nih.gov/geo/query/acc.cgi?acc=GSE167672).

In situ hybridization assays

Mouse brains were fresh-frozen in Tissue-Tek O.C.T. compound (Sakura) with dry ice and stored at -80 ºC until cryosectioning. Coronal sections (15 µm) containing the VN or the PBN were used for RNAscope (Advanced Cell Diagnostics) analysis following manufacturer's directions. The following probes were used: Mm-*Slc17a6* (#319171-C3), Mm-*Cck* (#402271-C2), Mm-*Crh* (#316091), Mm-*Fos* (#316921) and Mm-Calca (#578771-C2). All *in situ* hybridization assays were imaged using a confocal (Leica SP5) or epifluorescence (Nikon Eclipse 90i) microscope and analyzed in ImageJ (Fiji v1.0)

Statistics

Data are shown as the mean ± SEM. GraphPad Prism v9.0 software was used for statistical analyses. Appropriate tests were selected depending on the experimental design as stated in the figure legends. Statistical significance, when reached ($p<0.05$ was considered significant), is stated in the figure legends.

ACKNOWLEDGMENTS

Authors thank Diane Durnam for editing the manuscript. This work was supported by a NENS exchange grant for training stay (PMM), a Marie Sklodowska-Curie Individual Fellowship (H2020-MSCA-IF-2014-658352; ES), pre-doctoral fellowships (2018FI_B 00452

to AU; PRE2018-083179 to LSB) and two Ramón y Cajal fellowships (RyC-2012-11873; AQ, RYC2019-028501-I; ES). E.S received funds from MICIU Proyectos I+D+i “Retos Investigacion” (RTI2018-101838-J-I00). A.Q. received funds from the European Research Council (Starting grant NEUROMITO, ERC-2014-StG-638106), MINECO Proyectos I+D de Excelencia (SAF2014-57981P; SAF2017-88108-R), MICINN Proyectos I+D+i (PID2020-114977RB-I00), AGAUR (2017SGR-323) and “la Caixa” Foundation (ID 100010434), under the agreement LCF/PR/HR20/52400018.

AUTHOR CONTRIBUTIONS

RP, ES and AQ conceived, designed, and supervised the work. PMM, LSB, FM, AU, IA, ES and AQ acquired, analyzed, and interpreted the data. The manuscript was written by PMM, RP, ES and AQ and revised and edited by all authors.

COMPETING INTERESTS STATEMENT

The authors declare no competing interests.

REFERENCES

1. Bertolini, G. & Straumann, D. Moving in a Moving World: A Review on Vestibular Motion Sickness. *Frontiers in neurology* **7**, 14-14 (2016).
2. Graybiel, A., Wood, C.D., Miller, E.F. & Cramer, D.B. Diagnostic criteria for grading the severity of acute motion sickness. *Aerospace medicine* **39**, 453-455 (1968).
3. Money, K.E. Motion sickness. *Physiological Reviews* **50**, 1-39 (1970).
4. Nalivaiko, E. Thermoregulation and nausea. 445-456 (2018).

5. Previc, F.H. Do the organs of the labyrinth differentially influence the sympathetic and parasympathetic systems? *Neuroscience and biobehavioral reviews* **17**, 397-404 (1993).
6. Treisman, M. Motion sickness: an evolutionary hypothesis. *Science* **197**, 493-495 (1977).
7. Helling, K., Hausmann, S., Clarke, A. & Scherer, H. Experimentally induced motion sickness in fish: possible role of the otolith organs. *Acta oto-laryngologica* **123**, 488-492 (2003).
8. Ngampramuan, S.*, et al.* Thermoregulatory correlates of nausea in rats and musk shrews. *Oncotarget* **5**, 1565-1575 (2014).
9. Wei, X.*, et al.* Verification of motion sickness index in mice. *CNS neuroscience & therapeutics* **17**, 790-792 (2011).
10. Lackner, J.R. Motion sickness: more than nausea and vomiting. *Exp Brain Res* **232**, 2493-2510 (2014).
11. Bles, W., Bos, J.E., de Graaf, B., Groen, E. & Wertheim, A.H. Motion sickness: only one provocative conflict? *Brain Res Bull* **47**, 481-487 (1998).
12. Reason, J.T. Motion Sickness Adaptation: A Neural Mismatch Model. *Journal of the Royal Society of Medicine* **71**, 819-829 (1978).
13. Oman, C.M. Sensory conflict in motion sickness: an Observer Theory approach. *Pictorial communication in virtual and real environments*, 362-376 (1991).
14. James, W. THE SENSE OF DIZZINESS IN DEAF-MUTES. *American Annals of the Deaf and Dumb* **28**, 102-117 (1883).
15. Irwin, J.A. The pathology of sea-sickness. *The Lancet* **118**, 907-909 (1881).
16. Abe, C., Tanaka, K., Iwata, C. & Morita, H. Vestibular-mediated increase in central serotonin plays an important role in hypergravity-induced hypophagia in rats. *Journal of Applied Physiology* **109**, 1635-1643 (2010).
17. Murakami, D.M., Erkman, L., Hermanson, O., Rosenfeld, M.G. & Fuller, C.A. Evidence for vestibular regulation of autonomic functions in a mouse genetic model. *Proceedings of the National Academy of Sciences* **99**, 17078-17082 (2002).
18. Dieterich, M.*, et al.* Medial Vestibular Nucleus Lesions in Wallenberg's Syndrome Cause Decreased Activity of the Contralateral Vestibular Cortex. *Annals of the New York Academy of Sciences* **1039**, 368-383 (2005).
19. Angelaki, D.E. & Cullen, K.E. Vestibular system: the many facets of a multimodal sense. *Annu Rev Neurosci* **31**, 125-150 (2008).
20. Yates, B.J., Holmes, M.J. & Jian, B.J. Adaptive plasticity in vestibular influences on cardiovascular control. *Brain research bulletin* **53**, 3-9 (2000).
21. Yates, B.J. & Miller, A.D. Properties of sympathetic reflexes elicited by natural vestibular stimulation: implications for cardiovascular control. *Journal of Neurophysiology* **71**, 2087-2092 (1994).
22. Braun, J.J. & McIntosh, H. Learned taste aversions induced by rotational stimulation. *Physiological Psychology* **1**, 301-304 (1973).
23. Fuller, P.M., Jones, T.A., Jones, S.M. & Fuller, C.A. Neurovestibular modulation of circadian and homeostatic regulation: vestibulohypothalamic connection? *Proceedings of the National Academy of Sciences of the United States of America* **99**, 15723-15728 (2002).
24. Nalivaiko, E., Rudd, J.A. & So, R.H.Y. Motion sickness, nausea and thermoregulation: The “toxic” hypothesis. *Temperature: Multidisciplinary Biomedical Journal* **1**, 164-164 (2014).
25. Palmiter, R.D. The Parabrachial Nucleus: CGRP Neurons Function as a General Alarm. *Trends in neurosciences* **41**, 280-293 (2018).
26. Balaban, C.D. Vestibular nucleus projections to the parabrachial nucleus in rabbits: implications for vestibular influences on the autonomic nervous system. *Exp Brain Res*

108, 367-381 (1996).
27. Balaban, C.D. & Beryozkin, G. Vestibular nucleus projections to nucleus tractus solitarius and the dorsal motor nucleus of the vagus nerve: potential substrates for vestibulo-autonomic interactions. *Experimental brain research* **98**, 200-212 (1994).
28. Erö, C., Gewaltig, M.-O., Keller, D. & Markram, H. A Cell Atlas for the Mouse Brain. *Frontiers in Neuroinformatics* **12**, 84-84 (2018).
29. Abe, C.*, et al.* VGLUT2-expressing neurons in the vestibular nuclear complex mediate gravitational stress-induced hypothermia in mice. *Commun Biol* **3**, 227 (2020).
30. Holstein, G.R., Friedrich, V.L., Jr. & Martinelli, G.P. Glutamate and GABA in Vestibulo-Sympathetic Pathway Neurons. *Front Neuroanat* **10**, 7 (2016).
31. Gagliuso, A.H., Chapman, E.K., Martinelli, G.P. & Holstein, G.R. Vestibular neurons with direct projections to the solitary nucleus in the rat. *J Neurophysiol* **122**, 512-524 (2019).
32. Cai, Y.-L.*, et al.* Glutamatergic vestibular neurons express Fos after vestibular stimulation and project to the NTS and the PBN in rats. *Neuroscience Letters* **417**, 132-137 (2007).
33. Singh, P., Yoon, S.S. & Kuo, B. Nausea: a review of pathophysiology and therapeutics. *Therap Adv Gastroenterol* **9**, 98-112 (2016).
34. Ng, L.*, et al.* An anatomic gene expression atlas of the adult mouse brain. *Nature Neuroscience* **12**, 356-362 (2009).
35. Borgius, L., Restrepo, C.E., Leao, R.N., Saleh, N. & Kiehn, O. A transgenic mouse line for molecular genetic analysis of excitatory glutamatergic neurons. *Molecular and cellular neurosciences* **45**, 245-257 (2010).
36. Lidvall, H.F. Mechanisms of motion sickness as reflected in the vertigo and nystagmus responses to repeated caloric stimuli. *Acta Otolaryngol* **55**, 527-536 (1962).
37. Bolea, I.*, et al.* Defined neuronal populations drive fatal phenotype in a mouse model of Leigh syndrome. *Elife* **8** (2019).
38. Waespe, W. & Henn, V. The velocity response of vestibular nucleus neurons during vestibular, visual, and combined angular acceleration. *Exp Brain Res* **37**, 337-347 (1979).
39. Sanz, E., Bean, J.C., Carey, D.P., Quintana, A. & McKnight, G.S. RiboTag: Ribosomal Tagging Strategy to Analyze Cell-Type-Specific mRNA Expression In Vivo. *Curr Protoc Neurosci* **88**, e77 (2019).
40. Sanz, E.*, et al.* Fertility-regulating Kiss1 neurons arise from hypothalamic POMC-expressing progenitors. *J Neurosci* **35**, 5549-5556 (2015).
41. Sanz, E.*, et al.* Cell-type-specific isolation of ribosome-associated mRNA from complex tissues. *Proc Natl Acad Sci U S A* **106**, 13939-13944 (2009).
42. Parrott, R.F., Ebenezer, I.S., Baldwin, B.A. & Forsling, M.L. Central and peripheral doses of cholecystokinin that inhibit feeding in pigs also stimulate vasopressin and cortisol release. *Exp Physiol* **76**, 525-531 (1991).
43. Nijsen, M.J.*, et al.* The role of the CRH type 1 receptor in autonomic responses to corticotropin- releasing hormone in the rat. *Neuropsychopharmacology* **22**, 388-399 (2000).
44. Carter, M.E., Soden, M.E., Zweifel, L.S. & Palmiter, R.D. Genetic identification of a neural circuit that suppresses appetite. *Nature* **503**, 111-114 (2013).
45. Gallo, M., Marquez, S.L., Ballesteros, M.A. & Maldonado, A. Functional blockade of the parabrachial area by tetrodotoxin disrupts the acquisition of conditioned taste aversion induced by motion-sickness in rats. *Neuroscience letters* **265**, 57-60 (1999).
46. Chen, J.Y., Campos, C.A., Jarvie, B.C. & Palmiter, R.D. Parabrachial CGRP Neurons Establish and Sustain Aversive Taste Memories. *Neuron* **100**, 891-899 e895 (2018).
47. Campos, C.A.*, et al.* Cancer-induced anorexia and malaise are mediated by CGRP neurons in the parabrachial nucleus. *Nat Neurosci* **20**, 934-942 (2017).

48. Carter, M.E., Han, S. & Palmiter, R.D. Parabrachial calcitonin gene-related peptide neurons mediate conditioned taste aversion. *J Neurosci* **35**, 4582-4586 (2015).
49. Bernstein, I.L. Learned taste aversions in children receiving chemotherapy. *Science* **200**, 1302-1303 (1978).
50. Previc, F.H. Intravestibular Balance and Motion Sickness. *Aerosp Med Hum Perform* **89**, 130-140 (2018).
51. Kodama, T.*, et al.* Neuronal classification and marker gene identification via single-cell expression profiling of brainstem vestibular neurons subserving cerebellar learning. *J Neurosci* **32**, 7819-7831 (2012).
52. Lin, Y. & Carpenter, D.O. Medial vestibular neurons are endogenous pacemakers whose discharge is modulated by neurotransmitters. *Cellular and Molecular Neurobiology* **13**, 601-613 (1993).
53. Ris, L., Capron, B., Vibert, N., Vidal, P.P. & Godaux, E. Modification of the pacemaker activity of vestibular neurons in brainstem slices during vestibular compensation in the guinea pig. *Eur J Neurosci* **13**, 2234-2240 (2001).
54. Norris, A.J., Shaker, J.R., Cone, A.L., Ndiokho, I.B. & Bruchas, M.R. Parabrachial opioidergic projections to preoptic hypothalamus mediate behavioral and physiological thermal defenses. *Elife* **10** (2021).
55. Tan, C.L.*, et al.* Warm-Sensitive Neurons that Control Body Temperature. *Cell* **167**, 47-59 e15 (2016).
56. Roman, C.W., Derkach, V.A. & Palmiter, R.D. Genetically and functionally defined NTS to PBN brain circuits mediating anorexia. *Nat Commun* **7**, 11905 (2016).
57. Taniguchi, H.*, et al.* A resource of Cre driver lines for genetic targeting of GABAergic neurons in cerebral cortex. *Neuron* **71**, 995-1013 (2011).
58. Quintana, A.*, et al.* Fatal breathing dysfunction in a mouse model of Leigh syndrome. *J Clin Invest* **122**, 2359-2368 (2012).
59. Franklin, K.B.J. & Paxinos, G. *Paxinos and Franklin's The mouse brain in stereotaxic coordinates* (Academic Press, an imprint of Elsevier, Amsterdam, 2013).

FIGURES

Fig. 1: VGLUT2^{VN} neuron inactivation blocks rotation-induced kinetosis in mice. a, Mice were subjected to a rotational stimulus using a custom-made rotary device. Perpendicular distance from the mouse head to the axis of rotation was 5 cm. Mouse body inclination angle was 45º. **b**, Traveled distance during 60 min of open-field test after spin or control stimulation (n=6; Two-way ANOVA, P <0.001). **c**, Cumulative food intake after spin or control stimulation (n=6; Two-way ANOVA, P<0.01). Mice were food deprived for 24 h prior to the test. **d**, Body temperature difference (ΔT) after spin or control stimulation (n=5; Two-way ANOVA, P<0.01). **e**, *Slc17a6*^{Cre} mice were bilaterally injected in the vestibular

nuclei (VN) with AAV1-DIO-hM4Di·mCherry (Vglut2^{VN}:hM4Di mice) to inhibit glutamatergic neurons upon CNO administration. **f**, Total distance traveled during a 60-min open-field session after spin stimulation in CNO- or vehicle-injected Vglut2^{VN}:hM4Di mice (n=10; Two-way ANOVA, *P*<0.01). **g**, Cumulative food intake after spin stimulation in CNO- or vehicle-injected Vglut2^{VN}:hM4Di mice (n=7; Two-way ANOVA, *P*<0.001). Mice were food deprived for 24 h prior to the test. **h**, Body temperature difference (ΔT) after spin stimulation in CNO- or vehicle-injected Vglut2^{VN}:hM4Di mice (n=4; Two-way ANOVA, *P*<0.05). Arrow shows time of injection.

Fig. 2: VGLUT2^{VN} neuron activation is sufficient to induce kinetosis. a, *Slc17a6^{Cre}* mice were unilaterally injected in the right VN with AAV1-DIO-ChR2·YFP (Vglut2^{VN}:ChR2 mice) or AAV1-DIO-YFP (Vglut2^{VN}:YFP mice), followed by optical fiber implantation over the right VN to deliver 40-Hz, 10-ms, 10-mW, 473-nm light pulses for 5 min under different behavioral approaches. **b**, Traveled distance during 60 min of open-field test after photostimulation (Vglut2^{VN}:ChR2 mice n=7; Vglut2^{VN}:YFP mice n=5; two-way ANOVA, *P*<0.01). **c**, Normal-chow intake following laser onset in Vglut2^{VN}:ChR2 or Vglut2^{VN}:YFP mice. Animals were food-deprived for 24 h prior to photostimulation. (n=6; Two-way ANOVA, *P*<0.001). **d**, Water intake following laser onset in food-deprived, Vglut2^{VN}:ChR2 or Vglut2^{VN}:YFP mice (n=6; Two-way ANOVA, P<0.001). **e**, Highly palatable, chocolate-flavored drink intake following laser onset in food-deprived Vglut2^{VN}:ChR2 or Vglut2^{VN}:YFP animals (n=6; Two-way ANOVA, P>0.05).

f, Core body temperature difference (ΔT) in freely moving Vglut2^{VN}:ChR2 or Vglut2^{VN}:YFP mice after handling and laser stimulation (n=8; Two-way ANOVA, *P*<0.01). **g**, Core body temperature difference (ΔT) after photostimulation in restrained Vglut2^{VN}:ChR2 or Vglut2^{VN}:YFP mice (n=5; Two-way ANOVA, *P*<0.001). YFP: Vglut2^{VN}:YFP mice; ChR2: Vglut2^{VN}:ChR2 mice.

Fig. 3: Identification of VN glutamatergic subpopulations and their role in kinetosis. **a**, *Slc17a6*^{Cre} mice (n=3) were bilaterally injected in the VN with a viral vector expressing the RiboTag (AAV1-DIO-Rpl22HA) for the molecular profiling of VGLUT2^{VN} neurons. **b**, Differential expression analysis showing significant enrichment for candidate VGLUT2^{VN} neuron subpopulation marker transcripts in the immunoprecipitates of RiboTag assays when compared to inputs. Specific enrichment for *Slc17a6* (Vglut2), and depletion for inhibitory neuron (*Gad2*) and non-neuronal marker transcripts (*Cnp*, *Gfap*) were confirmed in the analysis (padj: adjusted *P*-value; FC: fold change). **c**, Double-label *in situ* hybridization assay (RNAscope) showing expression of *Crh* mRNA within *Slc17a6*-expressing cells. Scale bar: 100 µm. **d**, *Crh*^{Cre} mice were bilaterally injected in the VN with AAV1-DIO- hM4Di-mCherry (Crh^{VN}:hM4Di mice) to inhibit CRH^{VN} neurons upon CNO administration. **e**, Locomotor activity in Crh^{VN}:hM4Di mice after spin stimulation in CNO and vehicle-injected mice (n=9; Two-way ANOVA, $P>0.05$). **f**, Body core temperature difference (ΔT) in CNO or vehicle-injected Crh^{VN}:hM4Di mice after spin stimulation (n=4; Two-way ANOVA, $P>0.05$). Arrow shows time of injection. **g**, Double-label *in situ* hybridization assay (RNAscope) showing expression of *Cck* mRNA within *Slc17a6*-expressing cells. Scale bar: 100 µm. **h**, *Cck*^{Cre} mice were bilaterally injected in the VN with AAV1-DIO- hM4Di-mCherry (Cck^{VN}:hM4Di mice) to inhibit CCK^{VN} neurons upon CNO administration. **i**, 5-min open-field test in Cck^{VN}:hM4Di mice 30 minutes after CNO or vehicle administration (n=4; t-test, $P<0.01$). **j**, Open-field test in Cck^{VN}:hM4Di mice injected with CNO or vehicle after spin stimulation (n=4; Two-way ANOVA, $P<0.001$). **k**, Body core temperature difference (ΔT) in Cck^{VN}:hM4Di mice after CNO or vehicle administration (n=4; Two-way ANOVA, $P<0.001$). Arrow shows time of injection. **l**, Body core temperature difference (ΔT) in CNO or vehicle-injected Cck^{VN}:hM4Di mice after spin stimulation (n=4; two-way ANOVA, P-value<0.001). Arrow shows time of injection.

Fig. 4: Photoactivation of CCK^{VN} neurons induces kinetosis. a, *Cck^{Cre}* mice were unilaterally injected in the right VN with AAV1-DIO-ChR2·YFP (Cck^{VN}:ChR2 mice) or AAV1-DIO-YFP (Cck^{VN}:YFP mice) followed by an optical fiber implantation to deliver a 5-min, 473-nm laser stimulation (40-Hz, 10-mW, 10-ms pulses). **b**, Representative image at Bregma -6.0 mm showing ChR2·YFP and GFAP staining in a section containing the VN of Cck^{VN}:ChR2·YFP mice. GFAP staining revealed the optical fiber tract over the VN. **c**, Open-field test showing traveled distance after photostimulation in Cck^{VN}:ChR2 and Cck^{VN}:YFP mice (n=4; Two-way ANOVA, $P<0.01$). **d**, Normal-chow intake after light stimulation in Cck^{VN}:ChR2 and Cck^{VN}:YFP mice. Mice were food deprived for 24 h prior to stimulation (n=4; Two-way ANOVA, $P<0.05$). **e**, Body core temperature difference (ΔT) in Cck^{VN}:ChR2 and Cck^{VN}:YFP mice after handling and laser stimulation (n=4; Two-way ANOVA, $P<0.01$).

Fig. 5: VGLUT2^{VN} and CCK^{VN} neurons target the PBN. a, Illustration showing AAV1-DIO-Syn·GFP VN injection in *Slc17a6^{Cre}* mice for projection analysis of VGLUT2^{VN} neurons in the PBN. **b**, Representative image of Syn·GFP staining in the PBN of *Slc17a6^{Cre}* animals injected with AAV1-DIO-Syn·GFP in the VN. Scale bar: 800 µm. **c**, Schematic of AAV1-DIO-Syn·GFP injection in the VN of *Cck^{Cre}* mice for projection analysis of CCK^{VN} neurons in the PBN. **d**, Representative image of Syn·GFP staining in the PBN of *Cck^{Cre}* animals injected with AAV1-DIO-Syn·GFP in the VN. Scale bar: 800 µm. Panels b and d are from Bregma -5.2 mm to Bregma -5.34 mm. **e**, Illustration showing AAV1-DIO-ChR2·YFP or AAV1-DIO-YFP injection in the VN and optical fiber implantation over the PBN in *Cck^{Cre}* mice for photoactivation of CCK^{VN} neuron projections in the PBN (CCK$^{VN\rightarrow PBN}$). **f**, Open-field test showing traveled distance after CCK$^{VN\rightarrow PBN}$ photostimulation (n=4; Two-way ANOVA, $P>0.05$). **g**, Food intake in food-deprived mice after CCK$^{VN\rightarrow PBN}$ photostimulation (n=3; two-way ANOVA, P-value>0.05). **h**, Core body temperature difference (ΔT) after handling and

$CCK^{VN\rightarrow PBN}$ optogenetic stimulation ($Cck^{VN\rightarrow PBN}$:ChR2 mice n=3; $Cck^{VN\rightarrow PBN}$:YFP mice n=4; Two-way ANOVA, *P*>0.05).

Fig. 6: CCK^{VN} neuron projections to the PBN mediate conditioned taste aversion (CTA). a, Illustration depicting the cage used in the two-bottle CTA test. **b-f**, CTA response in mice exposed to a two-bottle-based test pairing a 5% sucrose solution to different stimuli including rotational stimulus (**b**) (n=4; t-test, P-value<0.001), optogenetic activation of CCK^{VN} neurons in Cck^{VN}:ChR2·YFP or control (Cck^{VN}:YFP) mice (**c**) (n=4; t-test, *P*<0.01), targeted optogenetic activation of the $Cck^{VN\rightarrow PBN}$ circuit in Cck^{VN}:ChR2·YFP (n=3) or control (Cck^{VN}:YFP; n=4) mice (**d**) (t-test, *P*<0.05), rotational stimulus in $Vglut2^{VN}$:hM4Di mice injected with CNO (n=4) or vehicle (n=3) (**e**) (t-test, *P*<0.001), or optogenetic activation of $VGLUT2^{VN}$ neurons in $Vglut2^{VN}$:ChR2·YFP (n=8) or control $Vglut2^{VN}$:YFP (n=6) mice (**f**) (t-test, *P*>0.05). **g**, Double-label *in situ* hybridization assay (RNAscope) at Bregma -5.2 mm showing expression of *Fos* mRNA within *Calca*-expressing neurons in the PBN of photostimulated Cck^{VN}:ChR2·YFP mice. Control mice were Cck^{VN}:YFP. Scale bar: 250 µm.

Fig. 7: A genetically defined model for vestibular-mediated neurobiological MS regulation. Inner ear stimuli, such as exposure to rotations, leads to the activation of $VGLUT2^{VN}$ neuronal subpopulations, mostly CCK^{VN}, leading to hypolocomotion, hypophagia, hypothermia and CTA development. Our results show that hypothermia and CTA are mediated by $CCK^{VN\rightarrow PBN}$ projections onto $CGRP^{PBN}$ neurons, while hypolocomotion and hypophagia are driven by different (yet to be identified) CCK^{VN} projections. We propose that CRH^{VN} neurons impinge onto CCK^{VN} neurons, while other $VGLUT2^{VN}$ subpopulations provide opposing effects, likely by activating local inhibitory neurons (gray neurons).

Extended Data Fig. 1: Effect of increasing rotational intensities and $VGLUT2^{VN}$

neuron chemogenetic inhibition on ambulatory activity in mice. a, Open field (OF) test showing reduced locomotor activity in mice subjected to rotational stimuli of different intensity and duration. Centrifugation at 234, 270 and 468 rpm produce a centrifugal force of 3, 4 (n=6) and 12 *g* (n=2), respectively (n=6; Two-way ANOVA, *P*<0.001). **b**, Representative image at Bregma -6.0 mm showing hM4Di·mCherry expression in the VN of Vglut2^{VN}:hM4Di mice. Scale bar: 800 µm. **c**, Spontaneous ambulatory activity of Vglut2^{VN}:hM4Di mice 30 min after CNO or vehicle administration in a 5-min, open-field test (n=10; t-test, *P*>0.05).

Extended Data Fig. 2: Increasing photostimulation frequencies decrease ambulatory activity in mice. **a**, Representative image at Bregma -6.0 mm showing ChR2·YFP and GFAP staining in a section containing the VN of Vglut2^{VN}:ChR2·YFP mice. GFAP staining reveals the optical fiber tract over the VN. Scale bar: 800 µm. **b**, Open field test showing traveled distance elicited by different unilateral photostimulation frequencies in Vglut2^{VN}:YFP and Vglut2^{VN}:ChR2·YFP mice.

Extended Data Fig. 3: CRH^{VN} neuron chemogenetic inhibition does not alter ambulatory activity, but photoactivation of CRH^{VN} neurons reduces ambulatory activity and decreases core body temperature. a, Locomotor activity in Crh^{VN}:hM4Di mice (in a 5-min, open-field session) 30 min after CNO or vehicle administration; (n=9; t-test, P>0.05). **b,** Crh-cre mice were unilaterally injected in the right VN with AAV1-DIO-ChR2·YFP (Crh^{VN}:ChR2 mice) or AAV1-DIO-YFP (Crh^{VN}:YFP mice) followed by an optical fiber implantation to deliver a 5-min, 473-nm laser stimulation (40-Hz, 10-mW, 10-ms pulses). **c**, Open-field test showing traveled distance after a 5-min photostimulation (40-Hz, 10-mW, 10-ms pulses) over the VN of Crh^{VN}:ChR2 mice (n=6) or Crh^{VN}:YFP mice (n=4). Two-way ANOVA, P<0.01. **d**, Body core temperature change in Crh^{VN}:ChR2 (n=6) and

Crh^{VN}:YFP (n=4) mice after handling and laser stimulation (Two-way ANOVA, P<0.001).

Extended Data Fig. 4: ChR2·YFP projections to the PBN and NTS in Cck^{VN}:ChR2·YFP mice. a-b, Representative images showing ChR2·YFP and GFAP staining in sections containing the PBN (a; at Bregma -5.2 mm) or the NTS (b; at Bregma -7.56 mm) of Cck^{VN}:ChR2 mice. GFAP staining evidence the optical fiber tract over the PBN in (a). DAPI is used as a nuclear counterstain. Scale bar: 800 µm (a); 400 µm (b).

Extended Data Fig. 5: *Fos* induction in CGRP PBN neurons after spin.
Double-label *in situ* hybridization assay (RNAscope) at Bregma -5.2 mm showing expression of *Fos* mRNA within *Calca*-expressing neurons in the PBN after rotational stimulation. Scale bar: 250 µm.

Fig. 1

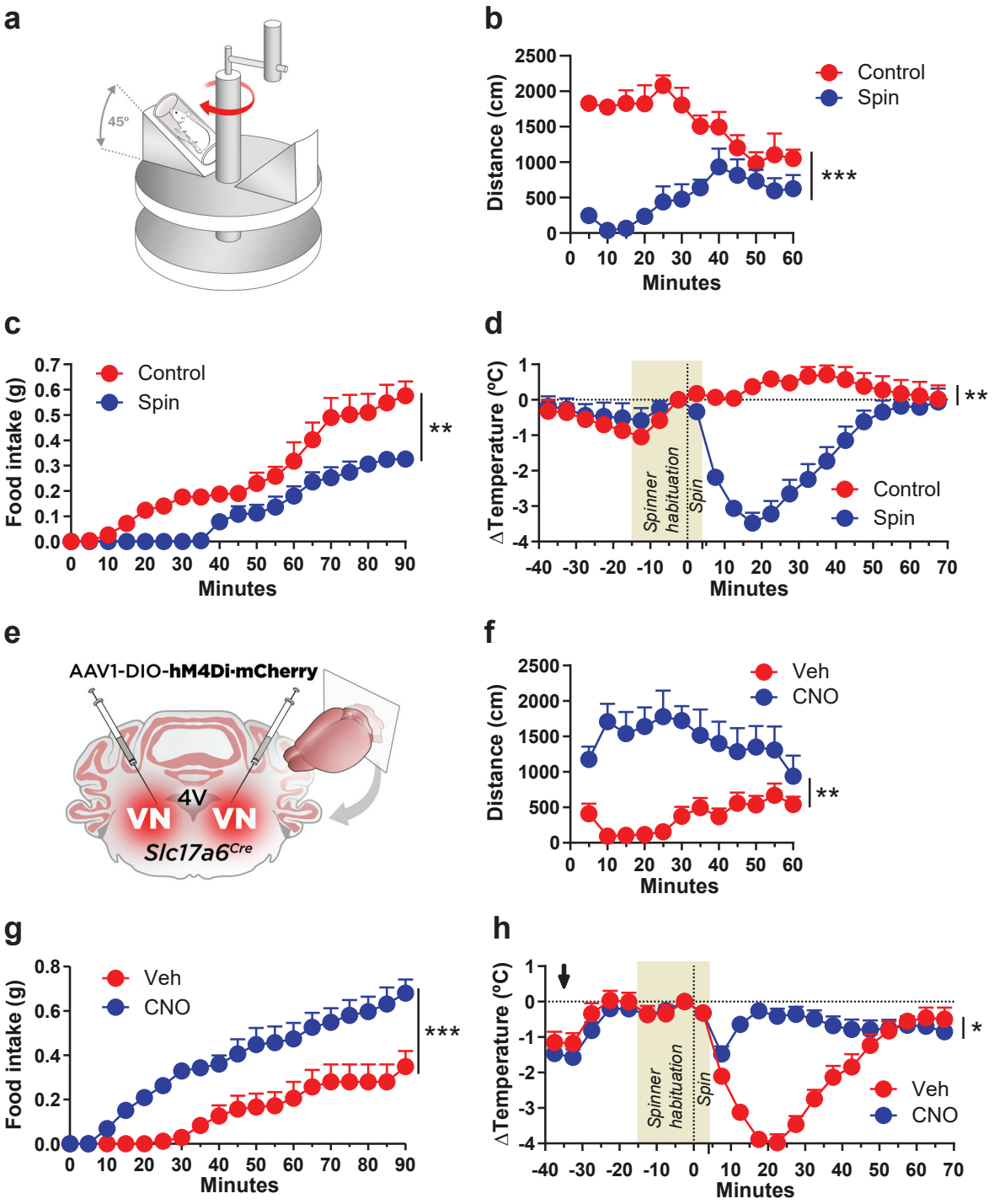
a
45°
b
Distance (cm)
Minutes
Control
Spin
***
c
Food intake (g)
Minutes
Control
Spin
**
d
ΔTemperature (°C)
Minutes
Spinner habituation
Spin
Control
Spin
**
e
AAV1-DIO-hM4Di-mCherry
4V
VN
VN
Slc17a6Cre
f
Distance (cm)
Minutes
Veh
CNO
**
g
Food intake (g)
Minutes
Veh
CNO
***
h
ΔTemperature (°C)
Minutes
Spinner habituation
Spin
Veh
CNO
*

Fig. 2

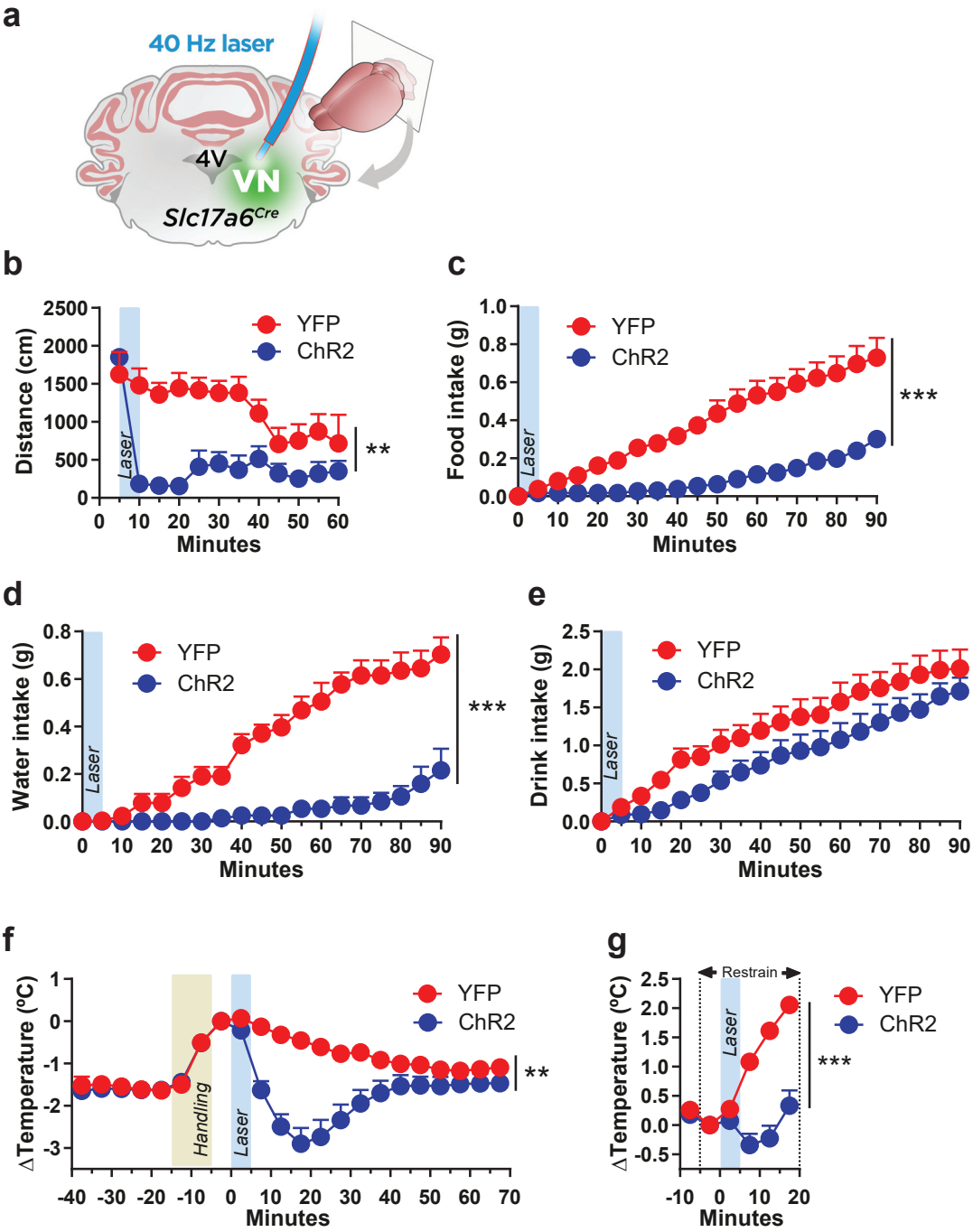
a
40 Hz laser
4V
VN
Slc17a6Cre
b
Distance (cm)
Minutes
YFP
ChR2
Laser
**
c
Food intake (g)
Minutes
YFP
ChR2
Laser
***
d
Water intake (g)
Minutes
YFP
ChR2
Laser
***
e
Drink intake (g)
Minutes
YFP
ChR2
Laser
f
ΔTemperature (ºC)
Minutes
YFP
ChR2
Handling
Laser
**
g
ΔTemperature (ºC)
Minutes
Restrain
YFP
ChR2
Laser
***

Fig. 3

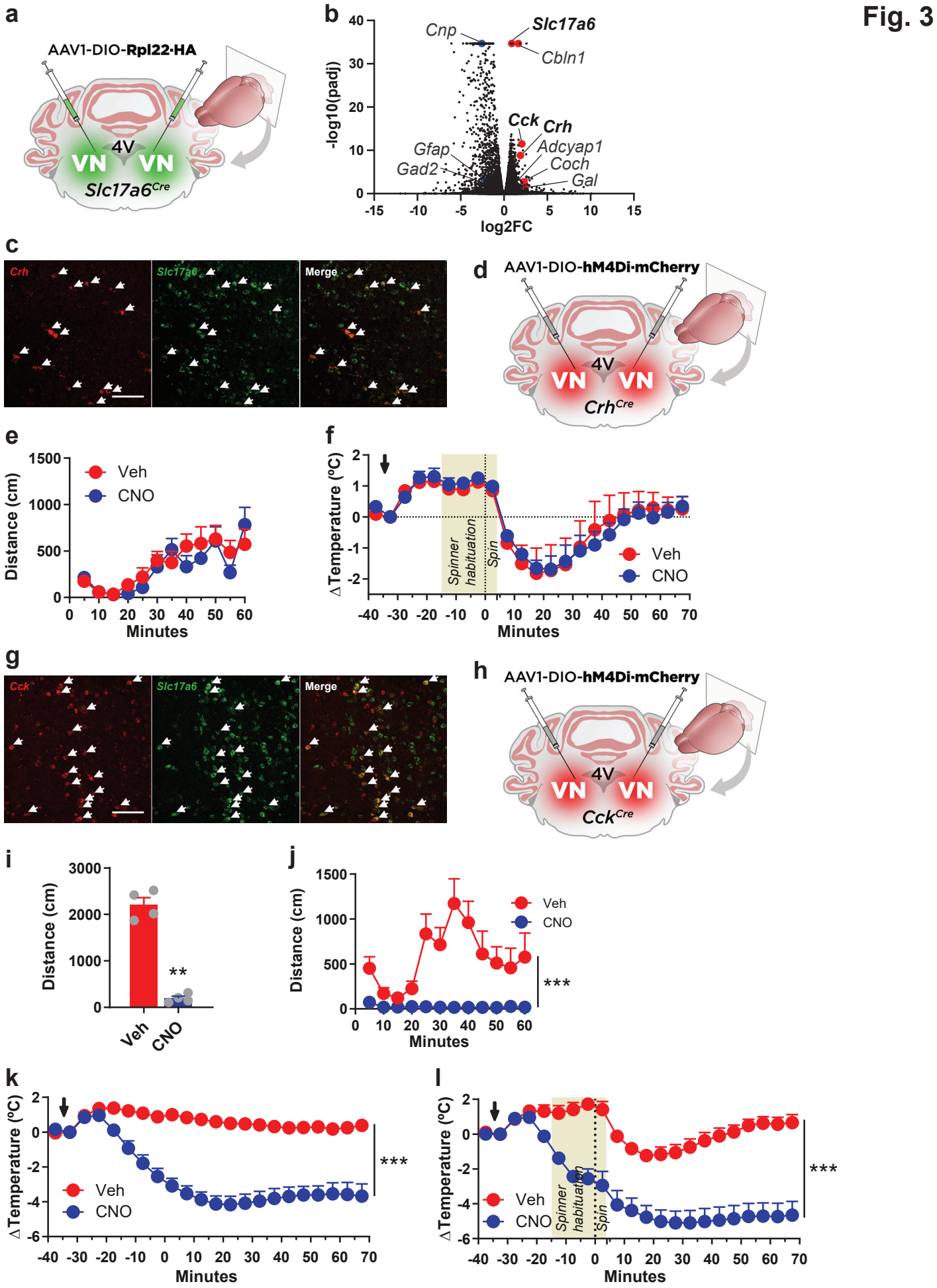
a
AAV1-DIO-Rpl22-HA
4V
VN
VN
Slc17a6Cre
b
-log10(padj)
log2FC
Cnp
Slc17a6
Cbln1
Cck
Crh
Adcyap1
Coch
Gal
Gfap
Gad2
c
Crh
Slc17a6
Merge
d
AAV1-DIO-hM4Di-mCherry
4V
VN
VN
CrhCre
e
Distance (cm)
Minutes
Veh
CNO
f
ΔTemperature (ºC)
Minutes
Spinner habituation
Spin
Veh
CNO
g
Cck
Slc17a6
Merge
h
AAV1-DIO-hM4Di-mCherry
4V
VN
VN
CckCre
i
Distance (cm)
**
Veh
CNO
j
Distance (cm)
Minutes
Veh
CNO
***
k
ΔTemperature (ºC)
Minutes
Veh
CNO
***
l
ΔTemperature (ºC)
Minutes
Spinner habituation
Spin
Veh
CNO
***

Fig. 4

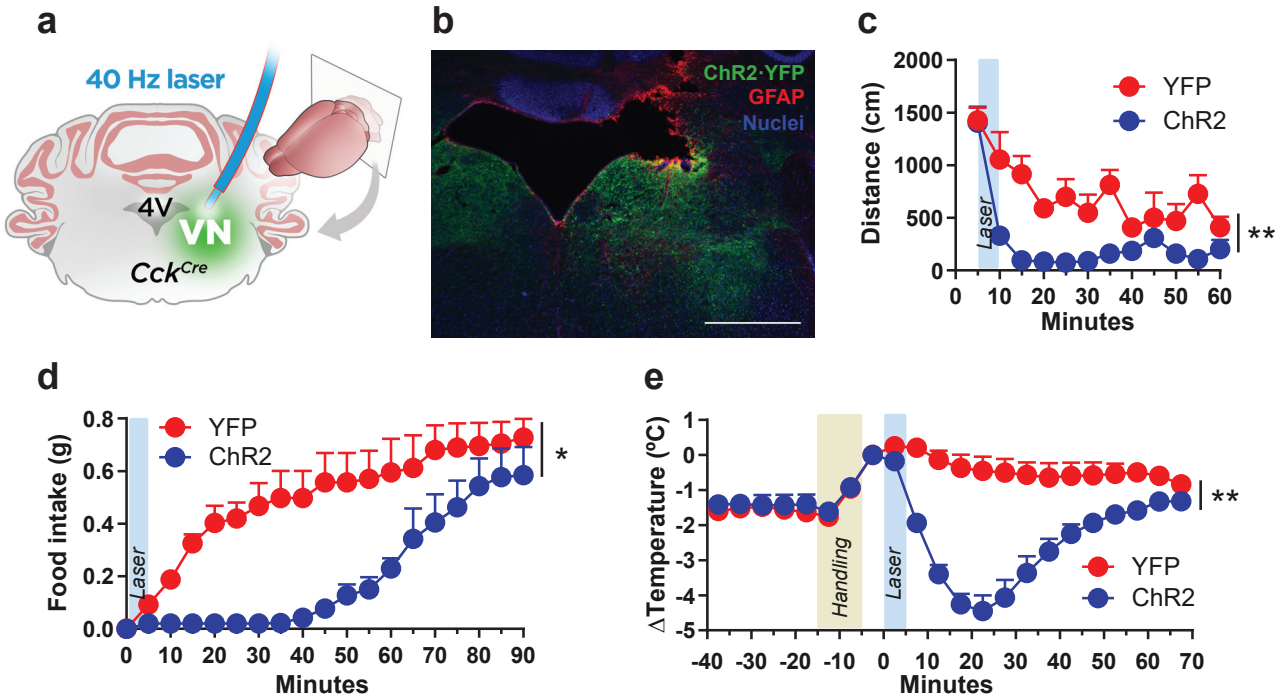
a
40 Hz laser
4V
VN
Cck^Cre
b
ChR2-YFP
GFAP
Nuclei
c
Distance (cm)
2000
1500
1000
500
0
Laser
YFP
ChR2
**
0 10 20 30 40 50 60
Minutes
d
Food intake (g)
0.8
0.6
0.4
0.2
0.0
Laser
YFP
ChR2
*
0 10 20 30 40 50 60 70 80 90
Minutes
e
ΔTemperature (ºC)
1
0
-1
-2
-3
-4
-5
Handling
Laser
YFP
ChR2
**
-40 -30 -20 -10 0 10 20 30 40 50 60 70
Minutes

Fig. 5

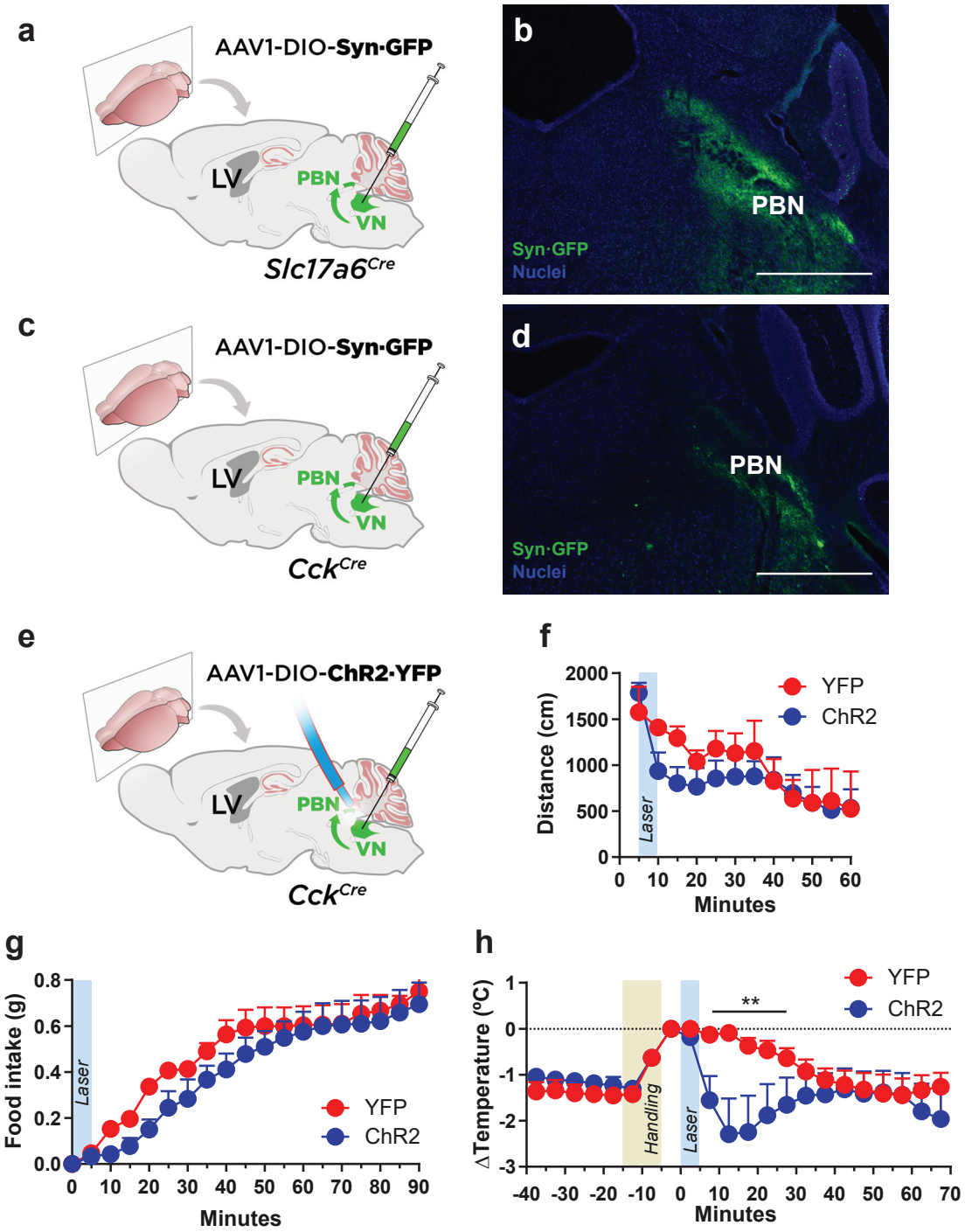
a
AAV1-DIO-Syn·GFP
LV
PBN
VN
Slc17a6Cre
b
PBN
Syn·GFP
Nuclei
c
AAV1-DIO-Syn·GFP
LV
PBN
VN
CckCre
d
PBN
Syn·GFP
Nuclei
e
AAV1-DIO-ChR2·YFP
LV
PBN
VN
CckCre
f
Distance (cm)
Minutes
Laser
YFP
ChR2
g
Food intake (g)
Minutes
Laser
YFP
ChR2
h
ΔTemperature (ºC)
Minutes
Handling
Laser
**
YFP
ChR2

Fig. 6

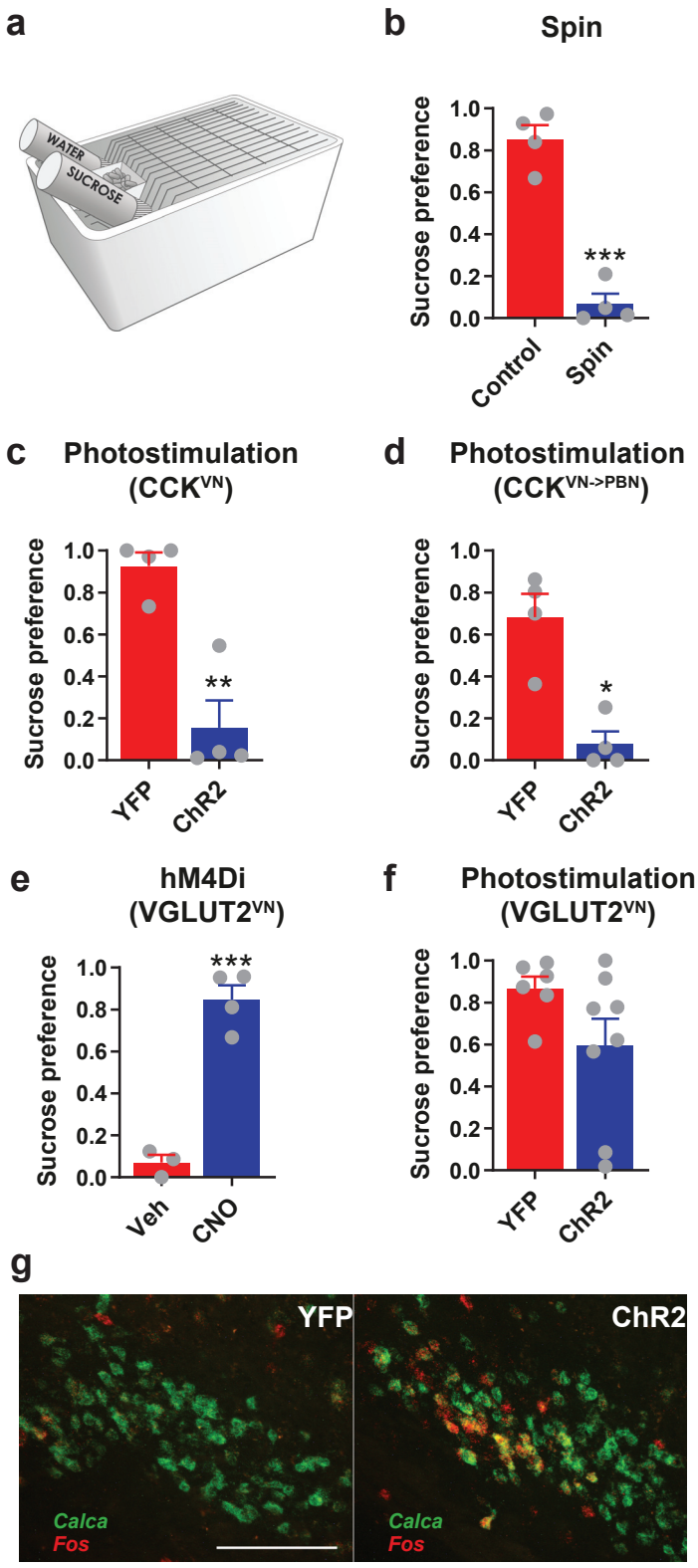
a
WATER
SUCROSE
b
Spin
Sucrose preference
1.0
0.8
0.6
0.4
0.2
0.0
***
Control
Spin
c
Photostimulation
(CCK^VN)
Sucrose preference
**
YFP
ChR2
d
Photostimulation
(CCK^VN->PBN)
Sucrose preference
*
YFP
ChR2
e
hM4Di
(VGLUT2^VN)
Sucrose preference
***
Veh
CNO
f
Photostimulation
(VGLUT2^VN)
Sucrose preference
YFP
ChR2
g
YFP
ChR2
Calca
Fos
Calca
Fos

Fig. 7

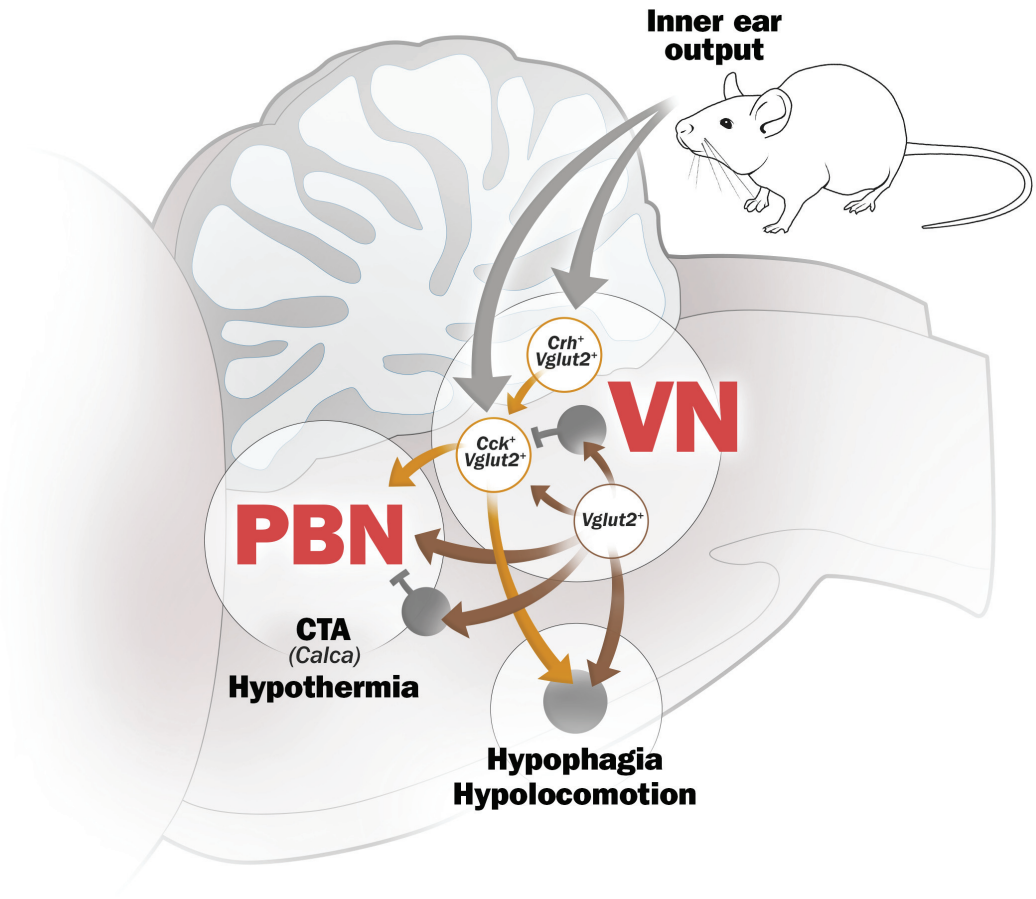
Inner ear
output
Crh+
Vglut2+
VN
Cck+
Vglut2+
Vglut2+
PBN
CTA
(Calca)
Hypothermia
Hypophagia
Hypolocomotion

Extended Data Fig. 1

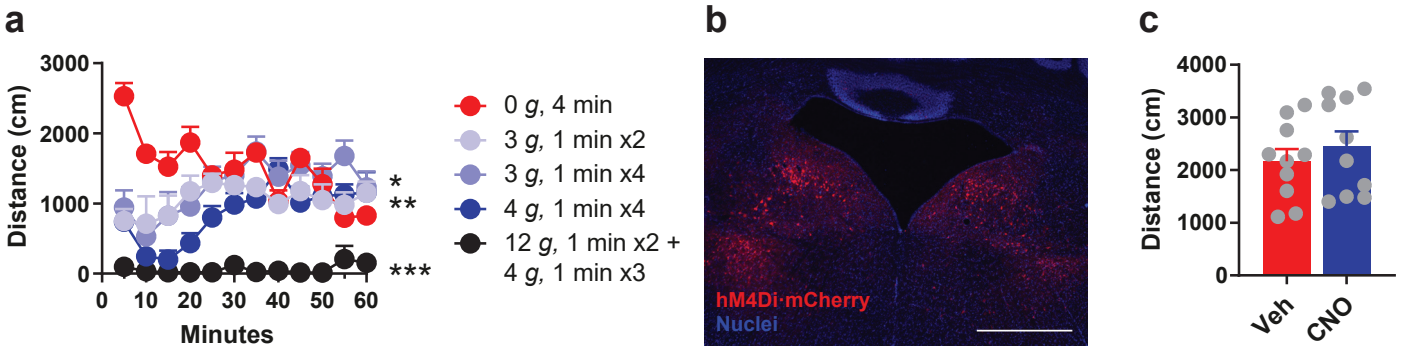

Extended Data Fig. 2

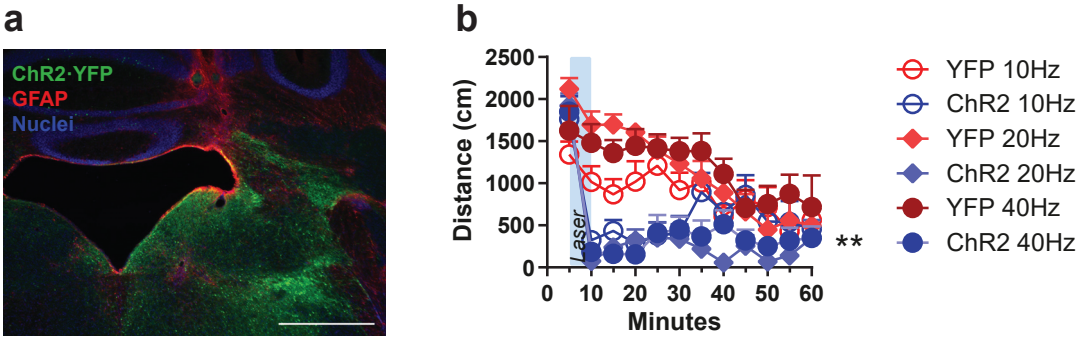

Extended Data Fig. 3

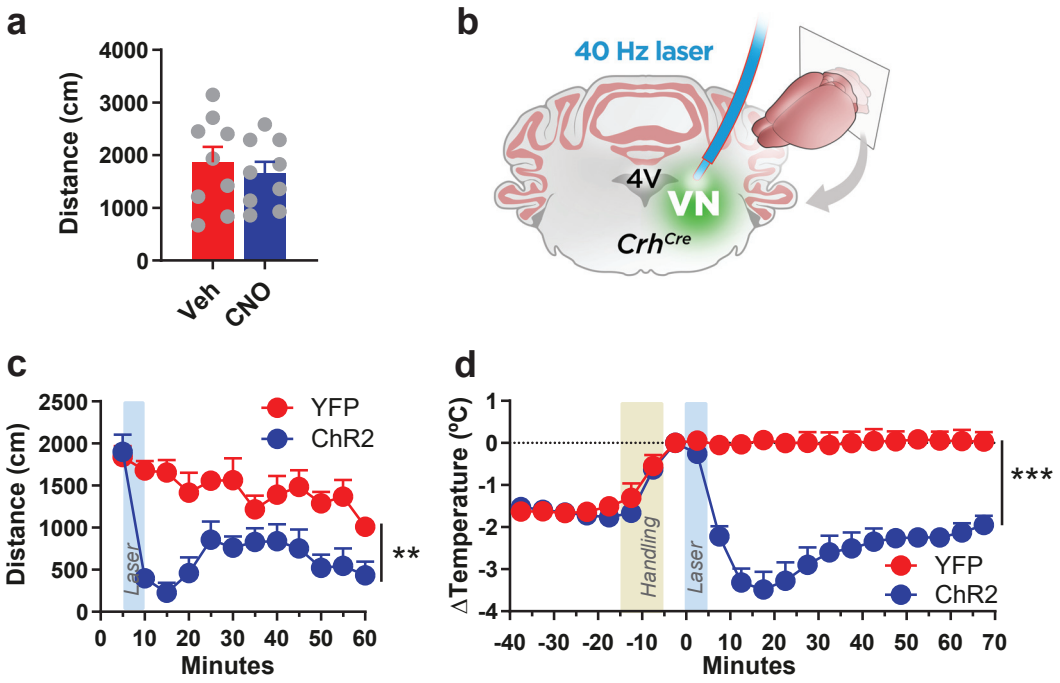

Extended data Fig. 4

a

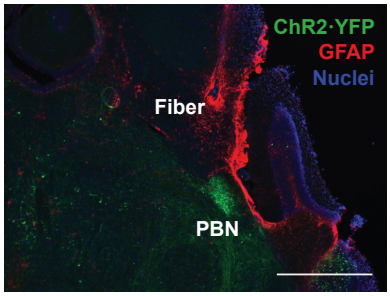

b

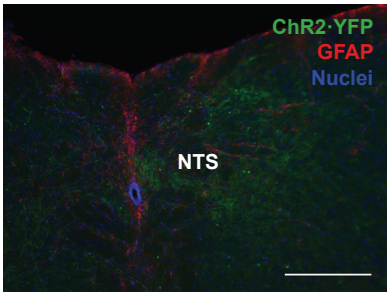
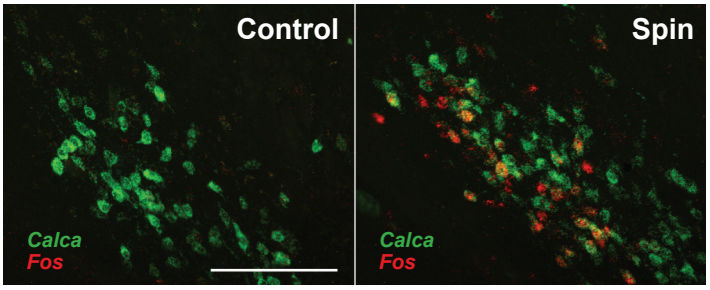
Extended Data Fig. 5